Potential energy surfaces for the interaction of CH(X2Π,B2Σ−) with Ar and an assignment of the stretchbend levels of the ArCH(B) van der Waals molecule

Millard H. Alexander, Susan Gregurick, Paul J. Dagdigian, George W. Lemire, Michael J. McQuaid et al.

Citation: J. Chem. Phys. **101**, 4547 (1994); doi: 10.1063/1.467442
View online: http://dx.doi.org/10.1063/1.467442
View Table of Contents: http://jcp.aip.org/resource/1/JCPSA6/v101/i6
Published by the American Institute of Physics.

Potential energy surfaces for the interaction of CH($X\,^2\Pi, B\,^2\Sigma^-$) with Ar and an assignment of the stretch-bend levels of the ArCH(B) van der Waals molecule

Millard H. Alexander and Susan Gregurick
Department of Chemistry and Biochemistry, University of Maryland, College Park, Maryland 20742-2021

Paul J. Dagdigian
Department of Chemistry, The Johns Hopkins University, Baltimore, Maryland 21218-2685

George W. Lemire,[a] Michael J. McQuaid,[b] and Rosario C. Sausa
US Army Research Laboratory, AMSRL-WT-PC, Aberdeen Proving Ground, Maryland 21005-5066

(Received 26 April 1994; accepted 31 May 1994)

New multireference, configuration-interaction potential energy surfaces are reported for the interaction of Ar with the CH radical in its ground ($X\,^2\Pi$) and second excited ($B\,^2\Sigma^-$) electronic states. These potential energy surfaces are then used in an adiabatic analysis of the rovibronic levels of the ArCH(X) and ArCH(B) van der Waals complexes. A qualitative discussion of the expected features in the $\tilde{B}\leftarrow\tilde{X}$ electronic spectrum of ArCH is presented, and these are compared with the experimental spectrum reported earlier by Lemire *et al.* [J. Chem. Phys. **99**, 91 (1993)].

I. INTRODUCTION

There has been considerable recent experimental interest in van der Waals complexes of argon with diatomic free-radical hydrides.[1] The molecules studied have included ArOH/D(X,A),[2–9] ArSH(X,A),[10] ArNH(a,c),[11] ArCH/D(X,B),[12,13] and ArBH(X,A).[14] For these systems the electronic spectrum of the complex, which occurs near electronic transitions in the free diatomic hydride, is interpreted to obtain information on the binding energy and structure of the complex. Theory can provide invaluable assistance in such investigations. *Ab initio* calculations of potential energy surfaces (PESs) can (and have) provided templates for the subsequent development of more refined, phenomenological PESs. Similarly, theoretical studies based on simplified, model descriptions of the interaction,[15–19] can lead to increased understanding of how the stretch-bend levels of the complex are reflective of the underlying PESs. Particularly successful examples of the contribution of theory are the work on ArOH of Clary, Lester, Bowman, Heaven, Hutson, and their co-workers,[20–24] based on the *ab initio* PESs of Degli-Esposti and Werner,[25] and our recent work on ArBH.[26]

In this paper we report a similar investigation of complexes of Ar with the CH radical. New *ab initio* calculations of the PESs for the interaction of Ar with CH in both its ground ($X\,^2\Pi$) and second electronically excited ($B\,^2\Sigma^-$) state, along with the subsequent determination of the bend-stretch levels of the ArCH(X,B) complexes, will be used to provide a more refined interpretation and analysis of the ArCH $\tilde{B}\leftarrow\tilde{X}$ spectrum, reported last year by Lemire *et al.*[12] The van der Waals complex of Ar with the $B\,^2\Sigma^-$ state of CH is, along with the complexes of Ar with the $A\,^2\Sigma^+$ state of OH,[8,20–22,25] inherently more simple than complexes involving diatomics in Π or Δ electronic states [as, for example, NH($c\,^1\Pi$)[11] or BH($A\,^1\Pi$)[14]] because only *one* electronic PES is necessary for the description of the interaction.[27]

To provide a theoretical framework with which to interpret the ArCH spectrum observed by Lemire *et al.*,[12] we present here multireference, configuration-interaction calculations of the PESs for the interaction of Ar with the CH radical in its ground ($X\,^2\Pi$) and second excited ($B\,^2\Sigma^-$) electronic states. We then use these potential energy surfaces in, first, an adiabatic bender[26] analysis and, second, a full variational determination of the rovibronic levels of the ArCH(B) van der Waals complex. The additional insight afforded by this theoretical investigation will allow us to interpret the high-resolution $\tilde{B}\leftarrow\tilde{X}$ electronic spectrum of the ArCH complex, in more detail than done in the original article of Lemire and co-workers.[12]

II. QUALITATIVE DISCUSSION OF ENERGY LEVELS

The nominal electron occupancies of the CH molecule in the $X\,^2\Pi$ and $B\,^2\Sigma^-$ states are $1\sigma^2 2\sigma^2 3\sigma^2 1\pi$ and $1\sigma^2 2\sigma^2 3\sigma 1\pi_x 1\pi_y$, respectively. The cylindrical degeneracy of the $X\,^2\Pi$ state will be lifted by approach of a collision partner, which will give rise to *two* electronic states, of A' and A'' symmetry (in C_s geometry).[28–33] For complexes of Ar with hydrides with a π^3 electron occupancy, for example ArOH($X\,^2\Pi$), the difference between the PESs corresponding to the A' and A'' electronic states is small[25] and can be accurately accounted for by a perturbation treatment.[16,17] By contrast, for complexes with hydrides with a π^1 electron occupancy [such as ArBH($A\,^1\Pi$)[26] or the present case of ArCH($X\,^2\Pi$)], our *ab initio* calculations indicate that the difference between the A' and A'' PESs is too large to be accommodated within a perturbation approach. For a full discussion of the theoretical treatment of van der Waals complexes of noble gas atoms with a diatomic hydride in a Π electronic state, we refer the interested reader to our earlier paper on the ArBH complex.[26] In the present paper we shall restate only the most relevant equations.

[a]Present address: Joint Contact Point Directorate, US Army Dugway Proving Ground, Dugway, UT 84022-5000.
[b]Present address: US Army Research Laboratory, AMSRL-WT-PA, Aberdeen Proving Ground, MD 21005-5066.

 0021-9606/94/101(6)/4547/14/$6.00

Approach of a spherical partner to the CH molecule in the B state, with electron occupancy $3\sigma 1\pi_x 1\pi_y$, will give rise to a single electronic state (Σ^- in linear geometry) of A'' reflection symmetry. As in a diatomic $^2\Sigma$ electronic state,[34] the electron spin is only weakly coupled to the molecular frame. Moreover, the spin splittings in ArCH($B\ ^2\Sigma^-$) are expected to be much smaller than for diatomic CH($B\ ^2\Sigma^-$), since they scale as the rotational constant.[6] Hence, we shall consider here only the spin-free energies of the van der Waals complex. Consequently, the ArCH($B\ ^2\Sigma^-$) bending and stretching motion can be interpreted with the theoretical treatments already developed and applied to a number of van der Waals complexes involving closed-shell diatoms.[35–39]

We follow the notation of earlier workers[16,40] and employ the labels K and P to denote, respectively, the spin-free projection along the intermolecular axis of the total angular momentum N *exclusive* of spin [for ArCH($B\ ^2\Sigma^-$)] and the projection of the total angular momentum J *inclusive* of spin [for ArCH($X\ ^2\Pi$)]. For the former electronic state, the coupling of the electron spin with N will give rise to a small spin splitting in the $K=0$ levels,[6] as in a diatomic $^2\Sigma$ electronic state. The similarly small spin splitting in the rotational energy level structure of the $K=1$ levels will be analogous to a diatomic $^2\Pi$ electronic state near the case (b) limit or in "nonunique" $K=1$ vibronic levels in a linear triatomic $^2\Pi$ Renner–Teller molecule.[40]

The rovibronic wave functions of the ArCH complex can be expanded in a basis involving either space-fixed (SF) or body-fixed (BF) diatom angular momentum wave functions.[16,26,39] In this paper, we explicitly neglect the vibrational motion of the diatomic CH. In the SF basis, we write the wave function for ArCH($X\ ^2\Pi$) as

$$\Psi^{JM}=(1/R)\sum_{jl\Omega\epsilon} C^J_{jl\Omega\epsilon}(R)|jl\Omega\epsilon;JM\rangle. \tag{1}$$

Here J designates the total angular momentum with space fixed projection M, l designates the orbital (end-over-end) angular momentum. The quantities j, Ω, and ϵ designate, respectively, the angular momentum, its projection on the internuclear axis, and the e/f symmetry[41] index of the rotational/fine-structure states of the CH($X\ ^2\Pi$) molecule ($\epsilon=+1$ for the e-labeled, and -1 for the f-labeled diatomic states.)[33] For the ArCH($B\ ^2\Sigma^-$) state, we designate the angular momentum of the diatom *exclusive* of the spin as n.

The functions $|jl\Omega\epsilon;JM\rangle$ in Eq. (1) are defined as

$$|jl\Omega\epsilon;JM\rangle=\sum_{m_j m_l}(jm_j lm_l|JM)Y_{lm_l}(\hat{R})\psi_{jm_j\Omega\epsilon}(\hat{r}), \tag{2}$$

where $(\cdots|\cdots)$ is a Clebsch–Gordan coefficient,[42] Y_{lm_l} is a spherical harmonic,[42] and $\hat{R}=(\Theta,\Phi)$ and $\hat{r}=(\beta,\alpha)$ designate the space-frame orientations of $\mathbf{R}$, the vector connecting the Ar atom and the diatom center of mass, and $\mathbf{r}$, the diatom (CH) internuclear axis. The symmetrized diatomic wave functions $\psi_{jm_j\Omega\epsilon}(\hat{r})$ in Eq. (2) can be written as

$$\psi_{jm_j\Omega\epsilon}(\hat{r})=2^{-1/2}[(2j+1)/4\pi]^{1/2}[D^{j*}_{m_j,\Omega}(\alpha,\beta,0)|\Lambda\Sigma\rangle + \epsilon D^{j*}_{m_j,-\Omega}(\alpha,\beta,0)|-\Lambda,-\Sigma\rangle], \tag{3}$$

where D^j_{mn} is a rotation matrix element,[42] and $\Omega=\Lambda+\Sigma$. Here $|\Lambda\Sigma\rangle$ designates the electronic wave function with Λ and Σ being the projections of the orbital and spin angular momenta, respectively, along the diatomic axis. The third Euler angle γ in Eq. (3) has been set to zero without loss of generality.[42,43] Because the parity of the $\psi_{jm_j\Omega\epsilon}(\hat{r})$ functions is $\epsilon(-1)^{j-S+s}$,[33,41] where S is the electron spin and s equals 1 for a Σ^- electronic state and 0 otherwise, and the inversion symmetry of the spherical harmonics is $(-1)^l$,[42] the total parity ($\pm$) of the $|jl\epsilon;JM\rangle$ functions is $\epsilon s(-1)^{j+l-S+s}$.

The expansion coefficients $C^J_{jl\epsilon}(R)$ satisfy the standard close-coupled (CC) equations.[33,39,44] The explicit form of the potential matrix in the SF basis has been given previously for the case of a diatomic molecule in both $^2\Pi$[33,45] and $^2\Sigma^+$[46] electronic state. For a $^2\Sigma^-$ state the expressions are identical to the latter case, except that the association of the parity to the symmetry index ϵ is *reversed*.

As an alternative to the SF expansion in Eq. (1), one can employ an expansion in the BF frame,[39,47–50] which is defined by the orientation of $\mathbf{R}$. In this case, the ArCH($X\ ^2\Pi$) wave function is expanded as follows:

$$\Psi^{JM}=(1/R)\sum_{jP\Omega\epsilon} C^J_{jP\Omega\epsilon}(R)|jP\Omega\epsilon;JM\rangle. \tag{4}$$

In Eq. (4), we have used the projection quantum number P inclusive of spin. The BF basis functions in Eq. (4) can be written as

$$|jP\Omega\epsilon;JM\rangle=2^{-1/2}[|jP\Omega;JM\rangle+\epsilon|jP,-\Omega;JM\rangle], \tag{5}$$

where the signed-Ω BF functions are given by[16]

$$|jP\Omega;JM\rangle=\frac{[(2j+1)(2J+1)]^{1/2}}{4\pi}D^{J*}_{M,P}(\hat{R})D^{j*}_{P,\Omega}(\hat{r}_b)|\Lambda\Sigma\rangle, \tag{6}$$

where $\hat{r}_b\equiv(\phi',\theta',0)$ denotes the orientation of $\hat{r}$ in the body frame.

For rovibrational states of ArCH($B\ ^2\Sigma^-$), we consider spin-free wave functions for the reasons discussed earlier and employ the spin-free projection quantum number K, instead of P. In this case the expressions for the SF and BF wave functions and potential matrix elements reduce to those for the interaction of a structureless atom with a closed-shell $^1\Sigma^+$ molecule,[44,48,49,51] except, as stated above, the parity labeling is *reversed* by the electronic wave function is Σ^-, as indicated by the paragraph after Eq. (3).

In both the SF and BF expansions, the matrix elements of the potential matrix are usually expressed as sums of terms $V_{\lambda 0}(R)$ and $V_{\lambda 2}(R)$, which arise in the expansion of the θ dependence of the PESs.[16,32,39,44,46] Specifically, $V_{\lambda 0}(R)$ and $V_{\lambda 2}(R)$ are the expansion terms of the *sum* and *difference* of the $V_{A'}$ and $V_{A''}$ PESs, namely

$$V_{\rm sum}(R,\theta)\equiv\frac{1}{2}\left[V_{A''}(R,\theta)+V_{A'}(R,\theta)\right]$$

$$=\sum_{\lambda=0}^{\lambda_{\max}} V_{\lambda 0}(R)P_{\lambda}(\cos\,\theta), \tag{7}$$

and

$$V_{\rm dif}(R,\theta)=\frac{1}{2}\left[V_{A''}(R,\theta)-V_{A'}(R,\theta)\right]$$

$$=\sum_{\lambda=2}^{\lambda_{\max}} V_{\lambda,2}(R)d^{\lambda}_{2,0}(\theta), \tag{8}$$

where $d^{\lambda}_{mn}(\theta)$ is a reduced rotation matrix element.[42] For the ArCH($B\,^2\Sigma^-$) complex, which is described in terms of only one PES, $V_{\rm dif}$ vanishes and Eq. (7) is just the expansion of this unique PES.

In the BF expansion, the potential matrix is block diagonal in P and independent of J.[33] However, the end-over-end rotational operator, which is diagonal and equal to $l(l+1)/2\mu R^2$ in the SF expansion, has both diagonal and off-diagonal terms in the BF basis.[39,52] The terms which couple different P blocks correspond to Coriolis coupling between the different BF projection states.

Rather than using the signed-P basis functions defined by Eq. (5), it is more convenient to use definite-P states, which correspond to states of well-defined parity, namely

$$|jP\epsilon\xi;JM\rangle=2^{-1/2}[|jP\epsilon;JM\rangle+\xi|j,-P\epsilon;JM\rangle], \tag{9}$$

where we have introduced the additional symmetry index $\xi=\pm1$. In the absence of Coriolis coupling, for a given magnitude of P, the eigenfunctions appear in degenerate pairs for $P\neq0$. The total parity ($\pm$) of the $|jP\epsilon\xi;JM\rangle$ functions in Eq. (9) is $\epsilon\xi(-1)^{J-S+s}$. We can define the e and f levels[41] of the complex as those for which $\epsilon\xi(-1)^s=+1$ and -1, respectively.

The present BF basis differs from that chosen by Dubernet *et al.*,[16] who define and label their basis functions by the *sign* of the product $P\Omega$. This is equivalent to employing the *signed*-Ω functions $|jP\Omega;JM\rangle$ instead of the symmetrized functions $|jP\epsilon;JM\rangle$ in the right-hand side of Eq. (9). We prefer the present BF basis since the symmetrization of the diatom wave function in Eq. (5) brings the diatomic rotational/fine-structure Hamiltonian closer to a diagonal form. Moreover, with a large difference potential $V_{\rm dif}$ [Eq. (8)], the ArCH wave functions are not well characterized by the product $P\Omega$, unlike the situation when $V_{\rm dif}$ is small.[16] The interaction $V_{\rm dif}$ breaks the cylindrical symmetry of the interaction potential since this term couples[33] different Ω states ($\Delta\Omega=\pm2$). Consequently, the symmetric and antisymmetric combinations of the $\pm\Omega$ states are a more appropriate basis.

By expansion of the wave function in either a BF or SF expansion, the energies and eigenfunctions of the bound states of the ArCH($X\,^2\Pi$,$B\,^2\Sigma^-$) complex can be obtained by determination of the $C^J(R)$ expansion coefficients. This can be done either variationally or by numerical solution of the CC equations.[39] More qualitative insight can be obtained by examination of the adiabatic potentials associated with the eigenvalues $w_{\rm ad}(R)$ of the Hamiltonian exclusive of the radial (Ar–CH separation) kinetic energy term. Since the BF and SF expansion states are related by an orthogonal transformation, the locally adiabatic states are identical regardless of whether the Hamiltonian is constructed in the BF or SF basis.

These radial adiabatic bender potentials can be used to investigate the vibrational motion along the van der Waals stretching coordinate R. The energies of these vibrational levels can be obtained by solution of a one-dimensional Schrödinger equation with potential $w_{\rm ad}(R)$. To the extent that off-diagonal matrix elements of the radial kinetic energy operator can be ignored, these energies will provide a good first approximation to the bound states of the ArCH complex. Such a Born–Oppenheimer separation of radial and angular motion in a van der Waals complex was first carried out by Holmgren *et al.*[53]

Since van der Waals complexes are so weakly bound, experimental studies are usually confined to supersonic nozzle preparation, and only states of low total angular momentum will have significant population. In this case, the Coriolis mixing between the various definite-P states, which varies approximately linearly with J,[29,39,49] will be small. In this case, additional physical insight can be gained by an examination of the definite-P adiabatic energies, obtained by diagonalization of a particular P-block of the Hamiltonian.

III. *AB INITIO* CALCULATIONS

To investigate quantitatively the energies of the ArCH complex, we carried out an *ab initio* determination of the PES for the single state of A'' reflection symmetry (in C_s geometry) which correlates with Ar+CH($B\,^2\Sigma^-$) and the two PESs for the states of A' and A'' reflection symmetry which correlate with Ar+CH($X\,^2\Pi$).

In most of the calculations reported here, we used the recent augmented correlation-consistent valence quadruple zeta (*avqz-f*) basis of Dunning and co-workers[27,54] with the exclusion of g functions on C and Ar and the exclusion of f functions on H ($13s7p4d3f$ contracted to $6s5p4d3f$ for C, $7s4p3d$ contracted to $5s4p3d$ for H, and $17s12p4d3f$ contracted to $7s6p4d3f$ for Ar). Some exploratory calculations were carried out with the smaller augmented correlation consistent triple zeta (*avtz*) basis[27,54] ($11s6p3d2\,f$ contracted to $5s4p3d2\,f$ for C, $6s3p2d$ contracted to $4s3p2d$ for H, and $16s10p3d2\,f$ contracted to $6s5p3d2\,f$ for Ar). The *avtz* and *avqz-f* bases contained of a total of 119 and 160 contracted Gaussian functions, respectively. All calculations were carried out with the MOLPRO suite of *ab initio* programs.[55] In all the calculations reported here, the CH bond distance was held to $r=1.377$ and $r=1.186$ Å, the experimental equilibrium bond lengths in the CH $X\,^2\Pi$ and $B\,^2\Sigma^-$ states, respectively.[56]

The interaction energy for each state can be defined as

$$V(R,\theta)=E_{\rm Ar\text{-}CH}(R,\theta)-\Delta E_{\rm CP}(R,\theta)-\Delta E_{\rm SC}(R,\theta)$$
$$-E_{\rm CH}(\infty)-E_{\rm Ar}(\infty). \tag{10}$$

Here the counterpoise correction, which adjusts for the lack of saturation of the orbital basis is defined by[57]

$$\Delta E_{CP}=E_{CH}(R,\theta)+E_{Ar}(R,\theta)-E_{CH}(\infty)-E_{Ar}(\infty) \quad (11a)$$

and the residual size consistency of the calculations is defined by

$$\Delta E_{SC}=E_{Ar\text{-}CH}(\infty)-E_{CH}(\infty)-E_{Ar}(\infty). \quad (11b)$$

In the determination of the PESs for the ArCH($X\ ^2\Pi$) complex we performed correlated electron pair (CEPA)[58–60] as well as complete-active-space self-consistent field (CASSCF)[61,62] calculations followed by multireference, internally contracted[63,64] configuration interaction (MRCI) calculations. In these latter calculations the active space in the CASSCF calculations was constructed by distributing the *six* valence CH electrons (all electrons exclusive of the C $1s$) among the *five* valence CH orbitals ($2\sigma,3\sigma,4\sigma,1\pi$).

For the calculations on the ArCH(X) complex the CASSCF orbitals were obtained by a state-averaging procedure[65–67] in which equal weights were assigned to the CH $X\ ^2\Pi_x$ and $X\ ^2\Pi_y$ states. In C_s geometry the reference space for the subsequent, internally contracted CI calculations consisted of 40 csf's for the states of $^2A'$ symmetry and 35 csf's for the states of $^2A''$ symmetry. The CI calculations included all single and double excitations out of this reference space with the exclusion of excitations out of the lower five orbitals of a', and the lowest orbital of a'', symmetry (which correspond to the C $1s$ orbital and the $n=1$ and $n=2$ shells of Ar). For the larger $avqz$-f basis this resulted in a total of 594 585 contracted (14 3645 525 uncontracted) configurations of A' symmetry and 507 123 contracted (14 3645 525 uncontracted) configurations of A'' symmetry. The contribution of higher-order excitations was then estimated using the internally contracted multireference version[68] of the Davidson correction [MR-CI(D)].[69]

For perpendicular ($\theta=90°$) approach of the Ar atom, Table I compares the ArCH(X) CEPA interaction energies determined with the $avtz$ and $avqz$-f bases, and the CEPA, MR-CI, and MR-CI(D) energies with the larger basis. We observe that the increased flexibility inherent in the larger $avqz$-f basis leads to only an extremely modest improvement in the calculated energies. Further, we see the CEPA and MR-CI(D) interaction energies agree quite closely. Since the CEPA calculations are far less computationally intensive, we used this method for the determination of the entire ArCH(X) PESs.

CEPA calculations were not possible for the ArCH($B\ ^2\Sigma^-$) complex, which is characterized by a triply open-shell ($3\sigma 1\pi_x 1\pi_y$) electron occupancy. Here, the state averaging in the determination of the CASSCF orbitals involved assigning equal weights to the two ground state configurations (CH $X\ ^2\Pi_x$ and $X\ ^2\Pi_y$) as well as to *all* the valence states which correspond to a $\cdots 3\sigma 1\pi^2$ electron occupancy ($A\ ^2\Delta_{xy}$, $A\ ^2\Delta_{x^2-y^2}$, $B\ ^2\Sigma^-_{xy}$, and $C\ ^2\Sigma^+_{x^2+y^2}$) states. For the $avqz$-f basis the number of contracted configurations consequently rose to 1 371 740 in the subsequent CI calculations for the state of A'' symmetry which corresponds to ArCH(B). Root flipping between the ArCH(B) and ArCH(A) states was found to occur at some geometries. Consequently it was necessary to search for both the second and third roots, simultaneously.

TABLE I. Comparison of calculated ArCH(X) PES for perpendicular approach of the Ar atom.[a]

R (bohr)	CEPA		MRCI	MRCI(D)
	$avtz$[b]	$avqz$-f[c]	$avqz$-f[c]	$avqz$-f[c]
		A' PES		
30.0[d]	0	0	4530.67	702.29
12.0	−5.04	−5.19	−4.02	−4.99
11.0	−8.72	−9.03	−7.18	−8.98
10.0	−15.66	−16.35	−12.99	−16.39
9.0	−28.40	−29.85	−23.22	−29.87
8.0	−45.82	−48.69	−34.97	−48.83
7.5		−52.16	−31.98	−52.32
7.0	−25.92	−32.87	−2.80	−33.13
6.5	63.37	51.81	97.07	49.61
6.0	322.61	303.66	373.43	300.26
5.5	985.16	954.94	1067.84	950.52
5.0	2563.30	2515.39	2706.08	2507.94
4.5	6138.70	6058.66		
		A'' PES		
30.0[d]	0.0	0.0	4543.74	729.18
12.0	−4.36	−4.47	−3.54	−4.31
11.0	−7.53	−7.73	−6.06	−7.37
10.0	−13.79	−14.14	−11.41	−13.89
9.0	−26.90	−27.50	−22.41	−27.34
8.0	−55.15	−56.36	−46.01	−56.63
7.5		−81.30	−66.03	−81.95
7.0	−111.60	−115.85	−93.30	−117.60
6.5	−149.85	−158.40	−124.62	−161.97
6.0	−178.83	−194.73	−144.06	−201.94
5.5	−148.49	−174.98	−98.42	−188.37
5.0	78.88	38.84	155.09	14.07
4.5	845.02	785.96	959.48	735.57

[a]Energies in cm^{-1}, distances in bohr.
[b]Augmented valence correlation-consistent triplet-zeta basis (Refs. 54 and 27).
[c]Augmented valence correlation-consistent quadruple-zeta basis (Refs. 54 and 27) *without* g functions on C and Ar and without f functions on H.
[d]Size consistency correction.

The major limitation in the present *ab initio* calculations is our inability to include in a precise manner the effect of higher order excitations. This drawback is particularly severe because we were unable to include in the active space any virtual excitations of the Ar electrons. Unfortunately, the virtual Ar orbitals lie considerably higher than many of the CH Rydberg orbitals. Thus, inclusion into the reference space of excitations of the Ar $3p$ electrons into higher Ar orbitals of s, p, and d symmetry, would so expand the active space as to render the calculations prohibitively time consuming.

MR-CI calculations of the ArCH(X) and ArCH(B) potential energy surfaces were carried out at seven values of θ (0°,30°,60°,90°,120°,150°,180°) and 11 values of the center-of-mass separation R (4.5, 5, 5.5, 6, 6.5, 7, 8, 9, 10, 11, and 12 bohr). For each value of θ the PESs were fit as a function of R to the general functional form[70]

$$V(R,\theta_i)=c_1\exp(-b_1R)+(c_2+c_3R)\exp(-b_2R)+c_4\{\tanh[1.2(R-R_0)]+1\}/R^6. \quad (12)$$

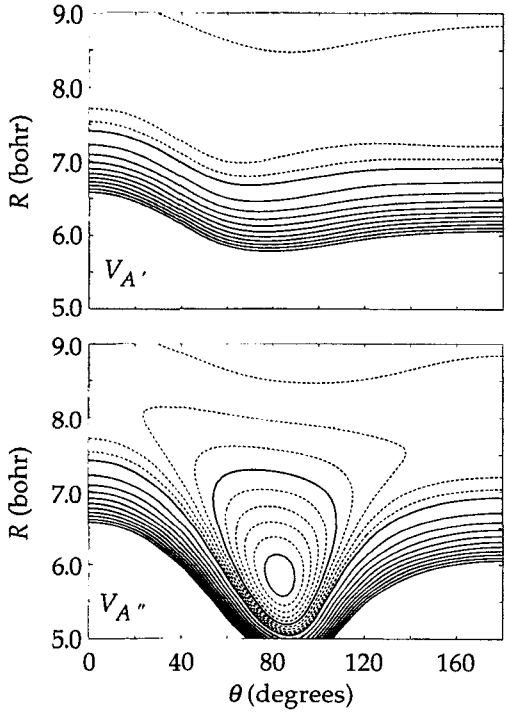

FIG. 1. Contour plots of the ArCH(X)PESs for the states of A' (upper panel) and A'' (lower panel) reflection symmetry. The linear CHAr geometry corresponds to $\theta=0°$. The dashed contours indicate negative energies with the first contour at -20 cm^{-1} and a spacing of 20 cm^{-1}. The solid contours designate positive energy; the contours are equally spaced with the first contour at 50 cm^{-1}, a spacing of 50 cm^{-1}, and the last (innermost) contour at 500 cm^{-1}. For clarity, the contours at 0, -100, and -200 cm^{-1} are drawn with heavy solid curves.

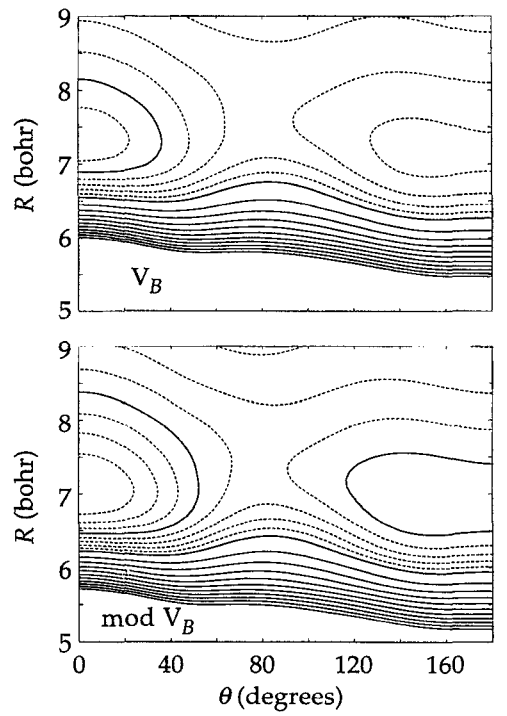

FIG. 2. Contour plot of the ArCH(B) PES (upper panel) and modified ArCH(B) PES (lower panel). The linear CHAr geometry corresponds to $\theta=0°$. The dashed contours indicate negative energies with the first contour at -20 cm^{-1}, a spacing of 20 cm^{-1}, and the last contour at -120 cm^{-1} (upper panel) and -160 cm^{-1} (lower panel). The solid contours designate positive energy; the contours are equally spaced with the first contour at 50 cm^{-1}, a spacing of 50 cm^{-1}, and the last (innermost) contour at 500 cm^{-1}. For clarity, the contours at 0 and -100 cm^{-1} are drawn with heavy solid curves.

The rms relative error in the fit was <0.1%. In the determination of the angular expansion coefficients in Eqs. (7) and (8) we took λ_{max} equal to 6, the upper limit imposed by the number of different values of θ at which *ab initio* calculations were carried out.

Figures 1 and 2 present contour plots of the PESs for the ArCH(X,B) electronic states. Table II lists the geometries of the minima and the dissociation energies. The equilibrium geometry of the ArCH(X) state is approximately T-shaped. Further, it is obvious from Fig. 1 that the ArCH(X) repulsive wall is quite anisotropic. The ArCH(X) PESs of A' and A'' symmetry are markedly distinct, reflecting the increased Pauli repulsion when the electron in the singly filled 1π orbital lies in the triatomic plane. Both PESs are qualitatively similar to those for ArBH(A)[26] where the electron occupancy the hydride ($\cdots 3\sigma 1\pi$) is also characterized by a singly filled π orbital. The A'' PES is significantly more attractive, with an approximately T-shaped equilibrium geometry. The A' PES possesses two shallow minima and has almost no barrier to internal rotation. Figure 3 displays the radial dependence of the angular expansion coefficients $V_{\lambda 0}(R)$ and $V_{\lambda 2}(R)$. The difference potential is dominated by just one term, $V_{22}(R)$, which indicates that the angular dependence of the difference potential is well modeled by $\sin^2\theta$. Consistent with the large difference in the ArCH(A)PESs of A' and A'' symmetry (see Fig. 2), the $V_{22}(R)$ term is comparable in magnitude to the largest anisotropy in the expansion of the average potential, $V_{20}(R)$.

By contrast, the ArCH(B) state has two minima, both in linear geometry. The deeper well corresponds to linear ArHC. As in the expansion of V_{sum} for ArCH(X), the angular expansion of the ArCH(B) PES is dominated by the $V_{20}(R)$ term. For the latter state, this term is *negative*, which reflects the preference for linear geometry. The ArCH(B) PES is

TABLE II. Equilibrium geometries and dissociation energies of ArCH.

State	θ_e	R_e (bohr)	D_e (cm^{-1})
		Ab initio PESs	
ArCH(X) $V_{A''}$	83.5	5.85	212
ArCH(X) $V_{A'}$[a]	51.5	7.65	60
	180.0	7.76	60
ArCH(B)	0	7.33	133
	150.0	7.17	87
		Modified PESs	
ArCH(X) $V_{A''}$	84.0	5.64	268
ArCH(X) $V_{A'}$[a]	53.0	7.41	78
	180.0	7.56	76
ArCH(B)	0.0	7.06	180
	150.5	6.90	119

[a]There are two minima on the A' ArCH(X) and ArCH(B) PESs; see Figs. 1, 2, 4, and 5.

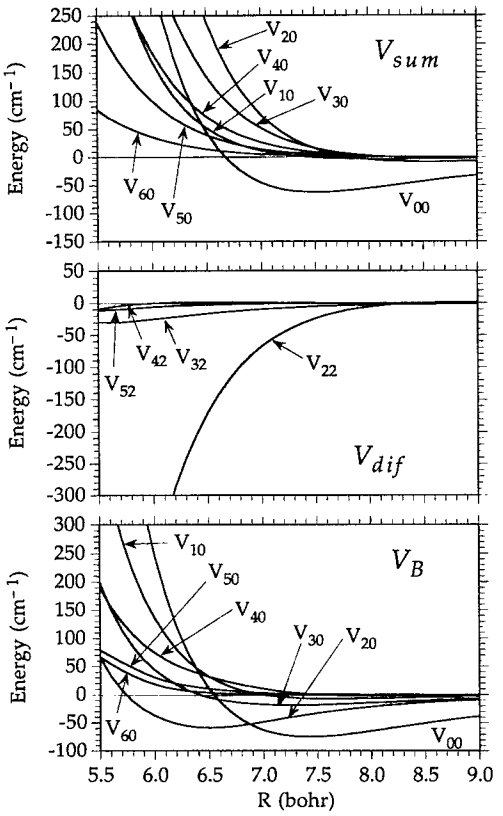

FIG. 3. Plots of the coefficients in the expansion in reduced rotation matrix elements of the CEPA ArCH(X) PESs and MR-CI(D) ArCH(X) PES. Upper panel: coefficients $V_{\lambda 0}(R)$ in the expansion of the average ArCH(X) potential [Eq. (7)]. Middle panel: coefficients $V_{\lambda 2}(R)$ in the expansion of the difference ArCH(X) potential [Eq. (8)]. The $\lambda=6$ term is extremely small and is not shown. Lower panel: coefficients $V_{\lambda}(R)$ in the expansion of the nondegenerate ArCH(B) potential.

qualitatively similar to that found for ArOH($A\ ^2\Sigma^+$),[25] and ArNH($c\ ^1\Pi$).[71] In all three cases the electron occupancy of the hydride [$\cdots 3\sigma 1\pi^2$ for CH(B), $\cdots 3\sigma 1\pi^3$ for NH(c), and $\cdots 3\sigma 1\pi^4$ for OH(A)] corresponds to a vacancy in the 3σ orbital which is normally doubly occupied in the ground electronic state.

Unfortunately, the similarity in the electron occupancy and angle corresponding to the van der Waals minimum cannot be extrapolated to the next member of this series, BH($A\ ^1\Pi$). Although the electron occupancy of the latter ($\cdots 3\sigma 1\pi$) has an identical vacancy in the 3σ orbital, the minimum occurs in *perpendicular* geometry.[26] Likely the minimum energy geometry in this later system is controlled by the singly filled 1π orbital, which exerts a strong preference for perpendicular geometry in the A'' state, rather than the singly filled 3σ orbital, which exerts a preference for linear geometry.

As a result of our inability to include higher order excitations involving the Ar electrons, we anticipate, based on our earlier investigation of the ArBH complex,[26] that the true CH–Ar van der Waals well depths will be ~50% deeper and the position of the minimum ~0.3–0.5 bohr closer in than predicted by our calculations. In our previous work on ArBH[26] we found that shifting and deepening the *ab initio* PESs in this manner led to a predicted zero-point corrected dissociation energy and rotational constant for the ground stretch-bend state of the ArBH(A) complex in much better agreement with the experimentally derived values[14] than the values predicted by the original *ab initio* PES. As discussed previously,[26] the calculated PESs could be deepened and contracted, without a qualitative change in the form of the PESs, by modifying the calculated $V(R,\theta_i)$ potential curves as follows:

$$V_{\rm mod}(R,\theta_i)=V(R+R_0,\theta_i)(1+0.5C\{\tanh[1.2(R-R_{ei}+R_1)]+1\}), \tag{13}$$

where R_{ei} is the position of the minimum of $V(R,\theta_i)$, and R_0, R_1, and C are constants, which are the same for all θ. At long range the transformation described by Eq. (13) increases the attractive tail of the potential by a factor of $(1+C)$. At short range the potential is translated inward by R_0 but otherwise unchanged. By a crude iterative comparison of adiabatic bender[26] predictions of the dissociation energies and rotational constants (see Sec. V A below) with the ArCH(X,B) dissociation energies we have derived from a reinterpretation (see Sec. VII) of the experimental spectra,[12] we adopted values of $R_0=0.32$ bohr, $R_1=0.37$ bohr, and $C=0.4$ for ArCH(X,B).

Contour plots of the modified ArCH PESs are shown in the lower panel of Fig. 2 [ArCH(B)] and Fig. 4 [ArCH(X)], and the equilibrium geometry and dissociation energies are listed in Table II. As can be seen in the comparison with the upper panel of Figs. 1 and 2, the modified PESs are deeper and shifted inward, but otherwise qualitatively unchanged. The angular expansion coefficients $V_{\lambda 0}(R)$ and $V_{\lambda 2}(R)$ for the modified PESs are qualitatively similar to those shown in Fig. 3 for the unmodified PESs, so, for brevity, are not shown. Figure 5 shows the dependence of the minimum energy path on the ArCH angle for the modified ArCH(XA''), ArCH(XA'), and ArCH(B) PESs. For the latter state, the barrier to internal rotation of the CH moiety is 104 cm^{-1}.

IV. CALCULATED BEND-STRETCH ENERGIES OF THE ArCH COMPLEX

A. Adiabatic bender energies

Definite-P and spin-free definite-K radial adiabatic bender potentials for ArCH(X) and ArCH(B), respectively, were calculated within the centrifugal decoupling (CD, also called "coupled-states") approximation.[52] In the CD approximation, the BF equations in the absence of Coriolis coupling are additionally modified by replacement of the true diagonal centrifugal barrier[29,49]

$$\hbar^2[J(J+1)+j(j+1)-2P^2]/2\mu R^2 \tag{14}$$

by the diagonal matrix[52,72]

$$\hbar^2\bar{l}(\bar{l}+1)/2\mu R^2, \tag{15}$$

where $\bar{l}$ is an effective angular momentum, taken the same for all channels. For the calculation of the asymptotic diatom rotational energies, the CH rotational constants and the $X\ ^2\Pi$ Λ doubling splitting parameters were taken from the

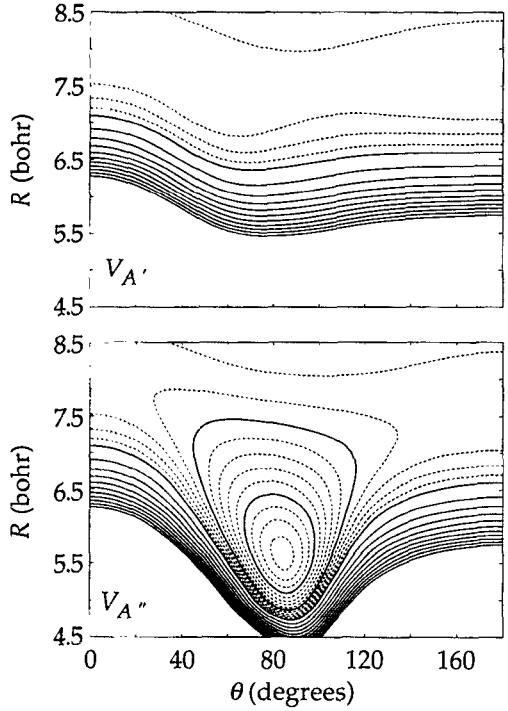

FIG. 4. Contour plots of the ArCH(X) PESs for the states of A' (upper panel) and A'' (lower panel) reflection symmetry, modified as described by Eq. (13). The linear CHAr geometry corresponds to $\theta=0°$. The dashed contours indicate negative energies with the first contour at -10 cm^{-1} and a spacing of 10 cm^{-1}. The solid contours designate positive energy; the contours are equally spaced with the first contour at 50 cm^{-1}, a spacing of 50 cm^{-1}, and the last (innermost) contour at 500 cm^{-1}. For clarity, the contours at 0, -100, and -200 cm^{-1} are drawn with heavy solid curves. Note that the ordinate is shifted by 0.5 bohr with respect to that in Fig. 1.

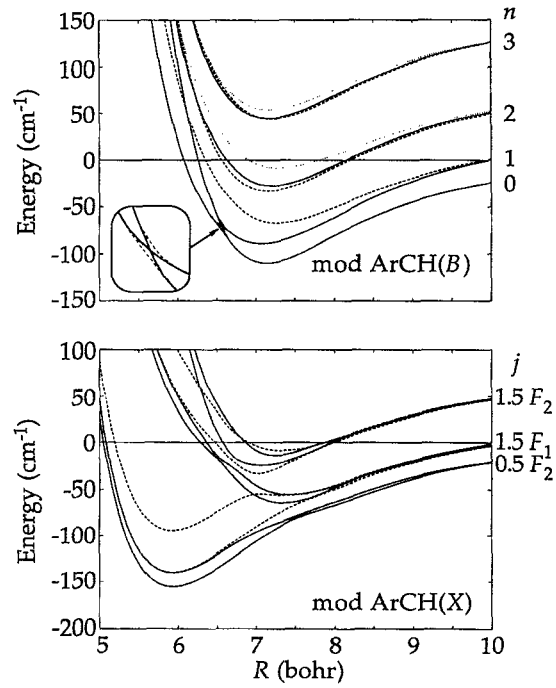

FIG. 6. Radial adiabatic bender potential energy curves for the ArCH system within the centrifugal decoupling approximation for an effective total angular momentum $\bar{l}=0$, determined using the *modified* PESs, within the spin-free treatment. The upper panel displays the adiabatic bender potentials for ArCH(B). The curves for $K=0$, 1, and 2 are denoted by, respectively, solid, dashed, and dotted lines. The correspondence of the asymptotes with the rotational levels of the CH($B\ ^2\Sigma^-$) diatom is indicated. In addition, although not shown for clarity, there will be two $K=3$ curves correlating with $n=3$. The inset in the lower left-hand corner of the upper panel illustrates the avoided crossing between the two lower $K=0$ curves. The lower panel displays the lower adiabatic bender potentials for ArCH(X). The $P=1/2$ and 3/2 adiabats are designated by solid and dashed lines, respectively, and the correspondence of the asymptotes with the rotational levels of CH($X\ ^2\Pi$) is indicated.

spectroscopic study of Bernath *et al.*[73] All calculations of the adiabatic potentials, for various values of the total angular momentum J, as well as the exact vibrational energies presented in Sec. V B below, were carried out with our Hibridon code.[74]

In interpreting the adiabatic curves, it is instructive to consider how the various terms in the interaction potentials influence the number and ordering of bender states. As discussed in Sec. II, by neglecting the small spin doubling in the

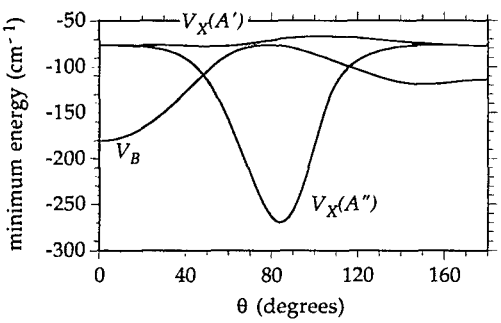

FIG. 5. Dependence of the energy (minimized with respect to R) as a function of the ArCH angle for the modified ArCH(X,A''), ArCH(X,A'), and ArCH(B) PESs.

CH $B\ ^2\Sigma^-$ state, we can analyze the pattern of these bender states by assuming the diatom to be in a closed-shell $^1\Sigma^+$ state. We follow Hutson's general analysis[36,39] and consider the low order $V_{\lambda 0}$ terms in the expansion of the ArCH(B) potential. For the lowest rotor asymptote ($n=0$) of a $^1\Sigma^+$ diatom, approach of a spherical partner gives rise to just one bender state with $K=0$. For the next rotor asymptote ($n=1$) there will be three bender states ($K=0$, $1e$, and $1f$), but in the absence of Coriolis coupling the $K=1$ e and f levels will be degenerate. Similarly, there will be three bender curves ($K=0,1,2$) for $n=2$. This is illustrated in the upper panel of Fig. 6, in which the calculated ArCH(B) CD bender curves are plotted.

It can be seen from Fig. 6 that splittings between the bender curves of different K correlating to the same rotor asymptote decrease with increasing n, reflecting the fact that the anisotropy of the potential has a smaller effect on the more rapidly rotating diatom. We see for the $n=1$ bender curves that the $K=0$ curve lies lower than the $K=1$ curve. To first order in perturbation theory, in which the diatomic rotational quantum number is a good quantum number, only the λ even ($V_{00}, V_{20}, \ldots$, terms) will effect the energies of the

adiabatic bender curves. Since the sign of V_{20} is negative in the region of the well in the isotropic potential (see Fig. 3), the $K=0$ adiabatic bender curve for $n=1$ lies lower than the $K=1$ curve. In fact, since the leading even anisotropy (V_2) will effect all levels *except* $n=0$ (to first order in perturbation theory) the $K=0$ adiabatic bender curve for $n=1$ actually diabatically crosses through the curve for $n=0$ and causes an avoided crossing in the adiabatic curves.

A similar avoided crossing in the lowest $K=0$ curve of the well-studied ArHCl($X\ ^1\Sigma^+$) complex appears as a local maximum in the dependence of the bender energy upon R.[53,75] This has been explained[53] as arising from the significant dependence of the equilibrium Ar–HCl separation upon the ArHCl angle. However, the variation in the positions of the two minima in the ArCH(B) PES (0.16 bohr, see Fig. 2 and Table II) is much smaller than the variation in the positions of the two ArHCl minima at linear geometries (~0.7 bohr, see Fig. 1 of Hutson[76]).

We further see in the upper panel of Fig. 6 that as n increases, the splitting between the $K=0$ and 1 adiabatic curves decreases. A higher degree of rotation of the CH moiety thus tends to reduce the ability of the CH moiety to sample the more attractive geometries of the ArCH(B) PES. We see, in addition, that the ordering of the ArCH(B) $K=0$ and 1 curves is reversed for $n=2$, as compared with $n=1$. This probably reflects the repulsion of the $K=0$ curve by the lower $K=0$ curves due to coupling between the underlying diabatic states.

The lower panel of Fig. 6 displays the lower $P=1/2$ and 3/2 bender curves for ArCH(X). It can be seen that there is a set of strongly bound bender curves, which all have their minima at $R\approx 5.9$ bohr. Additionally, there is a set of bender curves with much smaller binding energies and larger equilibrium CH–Ar separations. This pattern of bender curves is very similar to that for ArBH(A).[26] For both ArCH(X) and ArBH(A) the A' and A'' PESs are quite different, and $V_{\rm dif}$ is very large. As discussed by Alexander *et al.*[26] for ArBH(A), the strongly bound bender curves can be described as representing vibrational motion on the strongly bound A'' PES alone. For the weakly bound bender curves, there is considerable mixing of motion on the two PESs. Similar considerations apply to the strongly and weakly bound bender curves for ArCH(X). For the former, we see in Fig. 6 that the second $P=1/2$ and first $P=3/2$ bender curves are nearly identical in the region around the minima. These curves can be described as the two spin components of a spin-free $K=1$ bender curve. In like fashion, the lowest $P=1/2$ curve can be equated with a spin-free $K=0$ bender curve. Corresponding assignments of a spin-free projection quantum number K can be made for the higher strongly bound bender curves. The CH($X\ ^2\Pi$) spin–orbit splitting is quenched in the ArCH complex, so that the ArCH(X) spin splitting is small.

For brevity the CD adiabatic bender potentials derived from the unmodified ArCH(X,B) PESs are not displayed. They are qualitatively similar to those shown in Fig. 6, but a bit shallower with the minima shifted slightly toward larger internuclear distance. For the low rotational angular momenta sampled in the experiment of Lemire *et al.*,[12] the Coriolis coupling is so small that K (or P) is a nearly good quantum number for this system. The corresponding CC adiabatic bender potential curves are virtually identical to those shown in Fig. 6.

Within the adiabatic bender approximation, estimates of the stretch-bend energies of the complex can be obtained by numerical integration of the one-dimensional CD adiabatic bender potentials shown in Fig. 6. In particular Fig. 6 displays the avoided crossings between the $K=0$ ArCH(B) adiabats which correlate with $n=0$ and 1. Because these crossings are highly localized, the calculated adiabatic bender curves were first uncrossed (diabatized), as shown schematically in the upper panel of Fig. 6. For the modified PESs, the calculated adiabatic stretch-bend energies are listed in Table III. Also noted in Table III are the projection quantum number K and the CH(B) rotational level n to which the particular adiabatic bender potential correlates asymptotically. In addition, we label the energy levels in Table III with the vibrational quantum number of the Ar–CH van der Waals stretch motion. Since the experiments of Lemire *et al.*[12] provide information only on the ground vibrational level of ArCH(X), the calculated energy of this state alone is reported in Table III.

As in the case of ArBH(A),[26] because the adiabatic bender energies will be seen to be an excellent approximation to the full CC energies (see Sec. IV B), we advocate the use of this labeling scheme in assigning the observed levels of the ArCH complex, rather than other labeling schemes borrowed from those used for more rigid triatomics.[12,77,78]

The positions of the lower ArCH(B) bend-stretch levels for $K=0$ and 1 are illustrated pictorially in Fig. 7. It can be seen that the first $K=1$ bend-stretch level lies above the first three $K=0$ levels. There are a total of 13 bound bend-stretch levels supported by the modified ArCH(B) PES.[79] Also included in Table III, and illustrated in Fig. 7, are the calculated adiabatic energies for levels which lie above the dissociation limit and are supported by bender curves correlating to rotationally excited CH($n>0$)+Ar asymptotes.

Within the adiabatic bender model the Ar–CH motion is treated one dimensionally. For the calculated one-dimensional (in R) wave function one can calculate an effective ArCH rotational constant B, which is just proportional to $\langle R^{-2}\rangle$. We also present in Table III ArCH rotational constants calculated in this manner.

B. Exact ArCH vibrational energies

Finally, we present the results of exact calculations, using a spin-free basis (atom+$^1\Sigma^-$), of the vibrational levels of the ArCH(B) van der Waals complex, using the CC expansion of Eq. (1) and the CD approximation, with Eq. (4). For the latter calculations, and for CC calculations at a value of the spin-free total angular momentum $N=1$, a distributed Gaussian basis[80] was used to describe the expansion coefficients in Eq. (1). A total of 46 functions with an exponential parameter[80] A of 0.3 were used, equally positioned over the range $4\leq R\leq 18$ bohr. The required matrix elements over this Gaussian basis were obtained by numerical integration using a 560 point grid. Convergence to within less than 0.02 cm^{-1} could be obtained by including rotational states with $n\leq 9$ in the expansion.

TABLE III. Calculated low-lying energy levels (in cm^{-1}) of the ArCH(X) and spin–free ArCH(B) complexes, described by the modified PESs.

Adiabatic and CD															Full CC
$K=0$[a]					$K=1$					$K=2$ and 3[b]					$N=1$[c]
Adiab	B[d]	CD[e]	n[f]	v_s[g]	Adiab	B[d]	CD[e]	n[f]	v_s[g]	Adiab	B[d]	CD[e]	n[f]	v_s[g]	
							ArCH(X)[h]								
−131.8	0.167		0.5[i]	0											
							ArCH(B)								
−89.4	0.116	−88.8	0	0											−88.5
−71.3	0.119	−70.7	1	0											−70.3
−55.2	0.104	−54.2	0	1											−53.9
					−50.4	0.112	−47.5	1	0						−47.2
−40.0	0.111	−38.2	1	1											−37.7
−30.7	0.090	−29.7	0	2											−29.5
					−22.3	0.101	−19.2	1	1						−18.9
−14.5	0.099	−13.6	1	2											−13.5
					−14.4	0.115	−11.4	2	0						−12.0
−14.3	0.074	−12.4	0	3											−10.4
−9.6	0.114	−7.9	2	0											−7.1
−4.4	0.056	−3.8	0	4											−3.7
					−1.3	0.088	j	1	2						j
							$E=0$, Ar+CH($n=0$)								
4.4	0.099		1	3											
										7.0	0.111		2	0	
					13.1	0.073		1	3						
17.0	0.067		1	4											
					17.6	0.105		2	1						
21.3	0.104		2	1											
					21.7	0.054		1	4						
23.9	0.045		1	5											
							$E=25.3$, Ar+CH($n=1$)								
										33.6	0.099		2	1	
					41.9	0.092		2	2						
44.8	0.091		2	2											
										53.2	0.085		2	2	
					59.2	0.077		2	3						
61.3	0.076		2	3											
					62.5	0.114		3	0						
63.0	0.115		3	0											
										66.2	0.069		2	3	
					70.1	0.060		2	4						
										71.2	0.115		3	0	
71.4	0.057		2	4											
										73.5	0.048		2	4	
							$E=75.8$, Ar+CH($n=2$)								
										85.0[b]	0.110		3	0	
					94.3	0.104		3	1						
94.7	0.105		3	1											
										100.5	0.104		3	1	

[a]For $K=0$, the ArCH(B) $n=0$ and 1 curves were diabatized; see Fig. 6.
[b]The state with $E=85.0$ is the lowest state with $K=3$. All other energies in this column correspond to $K=2$.
[c]Close-coupled calculation in a spin-free (atom+$^1\Sigma^-$) basis.
[d]ArCH rotational constant (in cm^{-1}) predicted from adiabatic bender wave functions.
[e]Centrifugal decoupled calculations in spinless (atom+$^1\Sigma^-$) basis with $\bar{l}=0$.
[f]Correlation between the particular adiabatic bender potential and the asymptotic nuclear rotation quantum number of the separated CH molecule (see Fig. 6).
[g]van der Waals stretching quantum number.
[h]ArCH(X) calculations were carried out with the inclusion of the electron spin (atom+$^2\Pi$ basis).
[i]Asymptotic total angular momentum j of the separated CH($X\,^2\Pi$) molecule (see Fig. 6). For the ArCH(X) state, we have $P=1/2$ (projection quantum number inclusive of spin).
[j]No bound CD or CC states were found for this level.

Table III presents a full comparison between the calculated spin-free energies, as predicted by the adiabatic bender calculations discussed in the preceding section, those calculated within the centrifugal decoupling approximation (with a diagonal coupled states centrifugal barrier [Eq. (15)] with $\bar{l}=0$), and the full CC energies for a total angular momentum of $N=1$. We observe first a very good agreement between the adiabatic bender and CD energies. The differences are al-

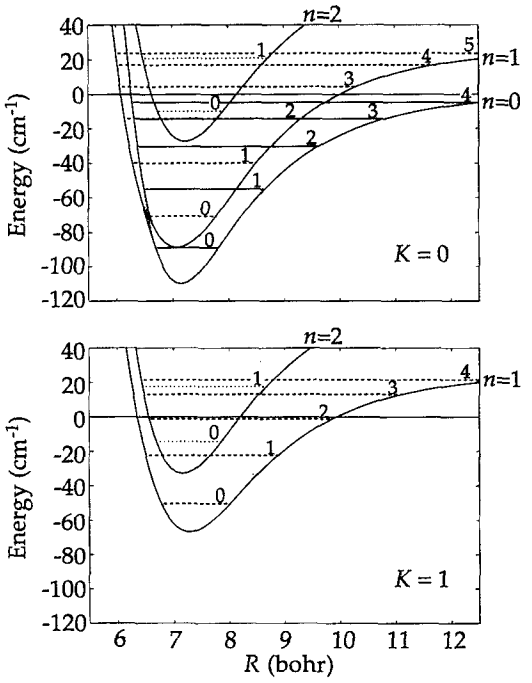

FIG. 7. Positions of the lower ArCH(B) van der Waals stretch levels (and vibrational assignments) determined from the $K=0$ radial adiabatic bender potential energy curves shown in Fig. 6. In the upper panel, the solid, dashed, and dotted lines correspond, respectively, to the stretch levels associated with the adiabatic bender curves which correlate, respectively, to $n=0$, 1, and 2 (see Fig. 6). (Lower panel) similar illustration of the van der Waals stretch levels determined from the $K=1$ radial adiabatic bender potentials. Again, the dashed and dotted lines correspond, respectively, to the stretch levels which correlate, respectively, to $n=1$ and $n=2$.

ways less than 1.9 cm^{-1}. This implies that the nonadiabatic corrections due to the crossings of the adiabatic curves in Fig. 6 will be small. The good agreement between the adiabatic bender, CD, and CC energies clearly justifies the assignment of each level within the adiabatic bender model in terms of the parentage of the particular adiabatic bender potential and the stretch vibrational quantum number.

V. PARITY SPLITTING IN THE GROUND ArCH(X) VIBRATIONAL LEVEL

As discussed previously,[17,39,81] in the absence of Coriolis coupling the rovibrational levels appear in degenerate pairs.

TABLE IV. Adiabatic bender energies[a] and parity splittings (in cm^{-1}) of the ground bend-stretch ArCH($X\ ^2\Pi$) vibrational level as a function of J.

	Adiabatic energy		
J	e	f	Splitting[b]
0.5	−131.556	−131.864	−0.308
2.5	−129.839	−130.761	−0.921
4.5	−126.726	−128.257	−1.531
6.5	−122.218	−124.351	−2.133
8.5	−116.332	−119.050	−2.718

[a]Calculated using CC bender curves.
[b]The sign of the splitting is defined as negative if the energy of the f level is less than that of the e level of the same J.

Green and Lester[17] and Dubernet *et al.*[18] have shown that the splitting ΔE of the definite $P=1/2$ levels of the same J but opposite parity should vary as $p(J+1/2)$. The magnitude of the splitting constant p should be directly proportional to V_{dif}, averaged over the van der Waals stretch vibrational wave function. Green and Lester[17] have derived an expression for p from third-order perturbation theory, in the limit of small V_{dif}. In fact, this splitting is analogous to the Renner–Teller splitting in $K=0$ vibronic levels of a linear triatomic $^2\Pi$ molecule, which is a direct measure of V_{dif}. Some years ago Hougen[40] showed how the splitting parameter p for these triatomic Renner–Teller systems can vary from $-2B$ to $+2B$. We follow Hougen's convention and define $\Delta E = E(J,f) - E(J,e)$.

For $p \approx 0$ [the case (a) limit], the rotational levels appear as closely spaced pairs of levels of the same J but *opposite* parity. However, when $|p| \approx 2B$ [the case (b) limit], the levels appear as closely spaced pairs of the *same* parity, with the same value of N, but with J differing by ± 1, analogous to the level structure of a diatomic $^2\Sigma$ state.[34] The lowest rotational level will have $J=1/2$ and $+(-)$ parity according to whether p is positive (negative). In the case (b) limit, the splitting between levels of the same N can be characterized a parameter γ. With some algebra, the case (b) spin splitting parameter γ can be expressed in terms of the case (a) parameter p as

$$\gamma = 2B + p \quad \text{for } p \approx -2B \ (^2\Sigma^- \text{ limit}), \tag{16a}$$

$$\gamma = 2B - p \quad \text{for } p \approx +2B \ (^2\Sigma^+ \text{ limit}). \tag{16b}$$

Lemire *et al.*[12] have observed a parity splitting in the ArCH $\tilde{B} \leftarrow \tilde{X}$ spectrum and ascribed this splitting to the ground state, since the spin splitting in the excited state is expected to be small.[6] Since the pattern of the bands was similar to that for a diatomic $^2\Sigma \leftarrow ^2\Sigma$ transition, the spectrum was analyzed by means of the usual case (b) rotational energy level formulas. Although the simulated spectra were not sensitive to the sign of γ for the lower state, the magnitude of the case (b) spin splitting parameter was found to be $|\gamma| = 0.021 \pm 0.004$ cm^{-1}. Since the upper state has $^2\Sigma^-$ symmetry, this implies that the lower state has the energy level pattern of a diatomic $^2\Sigma^-$ state.

For comparison, we can derive a theoretical estimate of the parity splitting in the lowest stretch-bend levels of the ArCH($X\ ^2\Pi$) complex. In Sec. V, we found that adiabatic bender energies generally provide a very good approximation to the exact energies. Accordingly, we have calculated adiabatic energies for the lowest stretch vibrational level ($v_s=0$) for a range of total J values and for both parities. In order to take Coriolis coupling into account, the bender curves were calculated by diagonalization of the full (CC) Hamiltonian. The calculated energies and parity splittings are displayed in Table IV. We follow the convention of Hougen[40] in Table IV and define the sign of the parity splitting as negative when the energy of the e level is greater than that of the f level. The calculated parity splittings are found to scale nearly perfectly with $(J+1/2)$. From a fit of the splittings we obtain a value of -0.302 cm^{-1} for the parameter p. From Eq. (16a), and using the theoretical rotational

constant of 0.167 cm^{-1} (Table III), we obtain a theoretical estimate of $\gamma = 0.032$ cm^{-1} for the case (b) splitting constant (the splitting between levels of the same N but with J differing by ± 1) for the ground bend-stretch level of ArCH($X\ ^2\Pi$). The agreement between this theoretical estimate and the experimental magnitude (0.021 ± 0.004 cm^{-1}; see above) is excellent, given that the calculated value of γ represents a difference [Eq. (16a)] between two numbers of nearly equal magnitude.

VI. COMPARISON WITH EXPERIMENTAL RESULTS AND DISCUSSION

In the analysis of their experimental spectra, Lemire *et al.*[12] derived estimates of the dissociation energies for ArCH(X,B). For bands associated with the CH($B,v=0$) vibrational level, they derived $D_0' \geqslant 172$ cm^{-1} from the wavenumber difference between the lowest-energy band (band A at 25 779 cm^{-1}) and the highest-energy observed feature (at 25 951 cm^{-1}). However, beyond their band G (at 25 859 cm^{-1}) the features are not rotationally resolved, indicative of broadening by predissociation. We would thus reinterpret their spectra and estimate $D_0' \geqslant 80$ cm^{-1}. With this estimate of the excited state dissociation energy $D_{0'}$ in hand, we can use the shift of band A from the diatomic CH transition [$^PQ_{12}(1)$ line at 25 698.23 cm^{-1}],[73] which connects the lowest-energy rotational levels in the X and B states, to estimate the ground state dissociation energy as $D_0'' \geqslant 161$ cm^{-1}. In similar fashion, bands correlating with the CH($B,v=1$) level do not show resolvable rotational structure beyond a newly observed band at 27 666 cm^{-1}, and we derive the estimate $D_0'(v=1) \geqslant 86$ cm^{-1}. We see that there is a significant dependence of the ArCH(B) dissociation energy on the CH diatom vibrational level. These estimates were used as a guide in modifying the *ab initio* ArCH(X,B) PESs, as described by Eq. (13).

Our calculated ArCH(B) vibrational energies, presented in Table III, can be used to confirm and extend the assignments made by Lemire *et al.*[12] of the observed ArCH $\tilde{B} \leftarrow \tilde{X}$ bands. Figure 8 presents a comparison of the experimentally observed energies for both ArCH($B,v=0$ and 1) with those calculated using the modified PES (Table III). For a shorthand description of the ArCH(B) vibrational levels, we utilize a notation similar to that employed by Heaven[1] for van der Waals complexes involving diatoms in Σ electronic states and denote the levels by (v,n^K,v_s).

Lemire *et al.*[12] observed 14 bands with well-resolved rotational structure, seven each associated with CH(B) $v=0$ and 1. The primary criteria for assigning the vibrational character of the bands were: (a) that the lowest observed transition was associated with the vibrationless ground level $(v,0^0,0)$, (b) that there would be a significant drop in the rotational constant B' for excitation in the stretching coordinate, and (c) that the level had $K=0$ if the rotational energy level structure of the upper level was well represented as a case (b) $^2\Sigma$ state. Complete vibrational quantum number descriptions for CH($B,v=0$) levels were proposed on the basis of these considerations: band A, $(0,0^0,0)$; band B, $(0,1^0,0)$; band C, $(0,0^0,1)$; and band E, $(0,0^0,2)$. Similarly, quantum numbers were assigned to two CH($B,v=1$) levels: band A, $(1,0^0,0)$, and band C, $(1,0^0,1)$. The vibrational energies and rotational constants calculated with the modified ArCH(B) PES are consistent with these assignments.

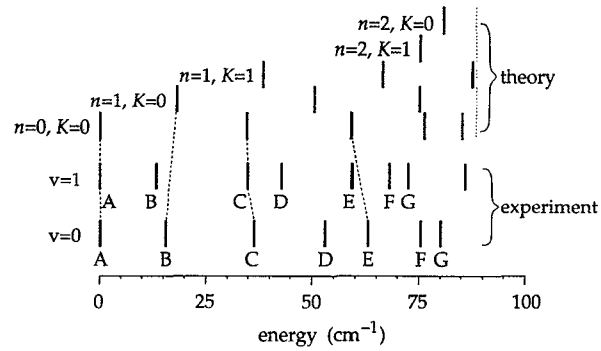

FIG. 8. Comparison of experimental vibrational energies for ArCH($B,v=0$ and 1) levels derived by Lemire *et al.* (Ref. 12) with calculated CD spin-free bend-stretch vibrational energies (Table III). The experimental and theoretical energies have both been shifted so that the lowest level has zero energy. The long vertical dashed line denotes the calculated dissociation limit. The short dashed lines illustrate the unambiguous spectral assignments made in Sec. VI.

The above assigned bands were the only spectral features which could be satisfactorily simulated through the application of simple $^2\Sigma$–$^2\Sigma$ transition formulas. Additional, incomplete vibrational assignments were tentatively proposed for CH($B,v=1$) bands B, E, and F, based on comparison with CH($B,v=0$) bands and partial rotational analyses. The $v=1$ band B was considered ascribable to $(1,1^K,0)$, but the assignment of K was uncertain. The energy separation between bands A and B was similar to that of the corresponding CH($B,v=0$) bands and suggests that $K=0$. However, the rotational structure was more complex than the corresponding $v=0$ band B. One possible explanation for the added complexity is that transitions to the $(0,1^0,0)$ and $(0,1^1,0)$ levels lie within 1–2 cm^{-1} of each other. The energy levels calculated with the modified ArCH(B) PES strongly suggest that the latter will be significantly higher in energy (by 23.2 cm^{-1}) than the former. It is possible, in principle, that either the anisotropy of the PES is greatly in error or that there is a very strong dependence of the anisotropy on the CH internuclear separation. However, we do not favor either of these explanations, and the upper level(s) associated with $v=1$ band B remain uncertain.

Partial rotational analyses of lines near the band heads of CH($B,v=1$) bands E and F yielded B' values of 0.099 cm^{-1}. This suggested that these bands were associated with $(1,1^K,1)$ levels, but again the incomplete nature of the rotational analysis prevented assignment of K. This result for band E is surprising since the $v=0$ band E is clearly assignable as a transition to $(0,0^0,2)$. In light of the present calculations, the rotational structure of $v=1$ band E was reexamined, but it was not possible to assign the spectrum to yield a B' value comparable to that for the corresponding $v=0$ band (0.086 cm^{-1}). Thus, the specific vibrational assignments of the $v=1$ bands E and F remain uncertain.

The only other features for which well-resolved rota-

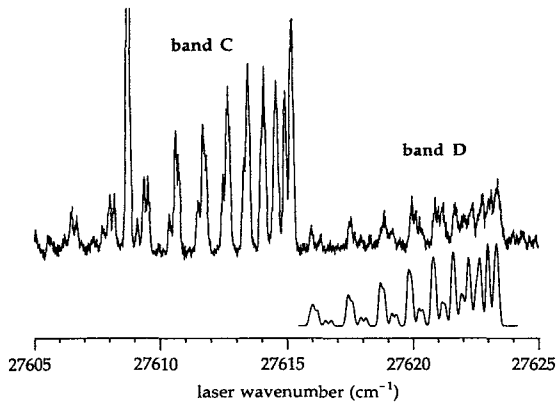

FIG. 9. Laser fluorescence excitation spectrum of bands C and D of ArCH associated with the CH $B-X$ (1,0) transition. The strong feature near 27 609 cm^{-1} is a diatomic transition. The lower trace displays a simulated spectrum of band D, assuming a $^2\Pi$(case b)$-^2\Sigma$ transition and an upper state rotational constant $B'=0.0955$ cm^{-1}.

tional structure was observed were the CH(B,$v=0$ and 1) bands D. (The latter band is displayed along with band C in Fig. 9.) Again, satisfactory simulations based on a simple $^2\Sigma-^2\Sigma$ model were not achieved; this suggests that this band does not involve a transition to a $K=0$ upper level. Comparison of the experimental and calculated energies (see Fig. 8) suggest a possible assignment, namely (v,1^1,0). In view of this possibility, we attempted to simulate the $v=1$ band D as a $^2\Pi$(case b)$-^2\Sigma$ transition. (A significant portion of the $v=0$ band D is overlapped with a diatomic CH $B-X$ line and could not be analyzed.) Simulations that were qualitatively better than those derived with a $^2\Sigma-^2\Sigma$ model were obtained; we compare in Fig. 9 the experimental spectrum with a simulation of this band using $B'=0.096\pm0.004$ cm^{-1}. This rotational constant, however, is considerably less than the value predicted (see Table III) for the (v,1^1,0) level (0.112 cm^{-1}). The low experimental B' value could be reconciled if, as discussed above, the $v=1$ band B involved a transition to the (1,1^1,0) level and band D, to (1,1^1,1), for which the rotational constant $B'=0.101$ cm^{-1} is predicted. Thus, we may reasonably assign $v=1$ band D as a transition to (1,1^1,v_s), but the specific value of v_s is uncertain.

We cannot assign to specific experimental bands the calculated levels which lie >60 cm^{-1} above the lowest level, (v,0^0,0). The energies, and indeed the number, of these levels is critically dependent on the assumed Ar–CH dissociation energy. Were this dissociation energy reduced by as little as 10 cm^{-1}, we see from Fig. 8 that many of the higher bend-stretch levels associated with the $n=0$ and 1 adiabats would become unbound.

In Table III we give the adiabatic energies of levels lying above the lowest Ar+CH(B) rotational asymptote. These levels, which are also displayed in Fig. 7, will be metastable and are subject to predissociation. Excitation to these levels will lead to bands with broadened rotational lines and hence unresolvable rotational structure. While we cannot provide a definitive assignment, the unresolved bands H through L in the spectra of Lemire *et al.*,[12] which are grouped within 90 cm^{-1} of our assumed dissociation energy, undoubtedly involve excitation to such predissociating levels.

We see that our calculated ArCH(B) vibrational energies have allowed us to confirm the assignments of the upper levels of the first four or five bands for $v=0$ and 1. There are, however, several as yet unresolved questions. As discussed above, we have been unable to deduce convincing assignments for the upper levels of the $v=0$ band D, the $v=1$ bands B, D and E, as well as the resolved bands of higher energy associated with both CH $v=0$ and 1. We see from Fig. 8 that the experimental ArCH(B) bend-stretch energies depend significantly on the CH diatom vibrational quantum number. This dependence likely reflects a significant dependence of the anisotropy of the PES. In view of our difficulties in assigning the experimental ArCH experimental spectrum, it would be desireable to investigate this dependence theoretically through further *ab initio* calculations in which the CH internuclear separation is varied. We note that the potential well associated with CH(B $^2\Sigma^-$) is shallow, and the vibrational frequency for this state is considerably smaller than for the X $^2\Pi$ and A $^2\Delta$ states.[56,73]

In support of our assignments and the present theoretical calculations, we note that the calculated splittings between the three stretch levels of the lowest ($n=0$) $K=0$ adiabat agrees remarkably well with experiment for CH(B,$v=0$) (bands A, C, and E; see Fig. 8). Further, the predicted rotational constants of bands A, B, C, and E (0.116, 0.119, 0.104, and 0.090 cm^{-1}) agree extremely well, both in absolute and relative magnitude, with the experimental values of Lemire *et al.*[12] (0.113, 0.116, 0.102, and 0.086 cm^{-1}). An interesting aspect of these rotational constants is that the B value for the (0,0^0,0) level is less than that for (0,1^0,0). This variation was also noted in our earlier spectroscopic studies of ArCH/D[12,13] and was interpreted to suggest that the H/D atom pointed away from the Ar atom. On the basis of the present study, this difference is attributable to differences in the averaging associated with the $n=0$ vs 1 bender curves, and not simple geometric considerations.

In related work, Heaven and co-workers[82] have assigned several bands in the NeCH/D $\tilde{B}\leftarrow\tilde{X}$ spectrum. The lowest B state levels identified correspond to the (0, 0^0, 0 and 1) levels as well as the (0,1^0,0) and (0,1^1,0) levels, similar to the four lowest ArCH levels (see Table III and Fig. 8). In the case of NeCH, the band involving the (0,1^0,0) level is broadened, an indication of predissociation. This then implies that the binding in the NeCH(B) complex is extremely weak, with $15.3<D_{0'}<23$ cm^{-1}. Because the (0,1^0,0) level lies below the corresponding $K=1$ level, Heaven and co-workers[82] conclude that the geometry of NeCH(B) is collinear, similar to ArCH(B). They further obtain vibrationally averaged values of the Ne–CH distance of 3.78 and 4.25 Å for the X and B state complexes. This should be contrasted with the case of ArCH, where we predict 3.23 and 3.87 Å, respectively. Despite the larger size of the Ar atom, the stronger attraction brings in the minima for the ArCH complex by approximately 0.4–0.5 Å. Finally, it would appear that the NeCH(B) PES is much less anisotropic than the ArCH(B) PES, since the barrier to internal rotation of the CH moiety found by Heaven and co-workers[82] is only 10.2 cm^{-1}, as

compared to our estimate (Sec. IV and Fig. 5) of 104 cm^{-1}.

VII. CONCLUSION

Our comparison with experimental data, and the more complete assignment of the experimental spectra achieved here, underscores the power of a joint theoretical-experimental investigation. In addition to presenting the results of sophisticated configuration-interaction calculations, which provide a template for the ArCH(X,B) PESs, this work has illustrated the usefulness of our adiabatic bender model. Here, the two-dimensional ArCH PESs are prediagonalized in the bending degree of freedom, which then provides a one-dimensional potential for the assignment and *quantitative* determination of the stretch-bend energies of the ArCH complex. Indeed, the slight errors in the adiabatic bender energies, when compared to more exact calculations based on the same PESs, are far less than the uncertainties in these PESs due to limitations in the treatment of dynamic electron correlation in our *ab initio* calculations.

The existence of substantial discrepancies, particularly with the higher bend-stretch levels of the ArCH(B) complex strongly suggest that further refinements of the ArCH(B) PES are necessary, along with additional experiments with higher spectral resolution. In addition, the dependence on the degree of vibrational excitation of the CH moiety of the spacing of the van der Waals stretching levels suggests that the ArCH(B) PES will vary significantly as a function of the CH bond stretch. This should be the object of future investigation. Notwithstanding, the overall satisfactory comparison with experiment shows clearly that *ab initio* calculations can provide an accurate template for the interaction of Ar with the CH radical.

ACKNOWLEDGMENTS

M.H.A., S.G., and P.J.D. wish to thank the US Army Research Office for support of the research reported here under Grant No. DAAL-03-91-G-0123. S.G. is also grateful for support under the DoD AASERT program. G.W.L., M.J.M., and R.C.S. wish to acknowledge support from the ARL Combustion Research Mission Program and the Productivity Capital Investment Program at ARL. G.W.L. is also grateful for support under the NRC-ARL Postdoctoral Associate Program. We also thank Michael Heaven for communicating the experimental results on NeCH from his laboratory. Some of the calculations reported here were supported by a grant of HPC time on the CRAY YMP-8 and C916 systems at the DoD HPC Shared Resource Center, U.S. Army Corp of Engineers Waterways Experiment Station, Vicksburg, MI.

[1] For a good recent review, see M. C. Heaven, J. Phys. Chem. **97**, 8567 (1993).
[2] M. T. Berry, M. R. Brustein, J. R. Adamo, and M. I. Lester, J. Phys. Chem. **92**, 5551 (1988).
[3] M. T. Berry, M. R. Brustein, and M. I. Lester, J. Chem. Phys. **90**, 5878 (1989).
[4] W. M. Fawzy and M. C. Heaven, J. Chem. Phys. **89**, 7030 (1988); **92**, 909 (1990).
[5] M. T. Berry, M. R. Brustein, M. I. Lester, C. Chakravarty, and D. C. Clary, Chem. Phys. Lett. **178**, 301 (1991).
[6] B.-C. Chang, L. Yu, D. Cullin, B. Rehfuss, J. Williamson, T. A. Miller, W. M. Fawzy, X. Zheng, S. Fei, and M. Heaven, J. Chem. Phys. **95**, 7086 (1991).
[7] B.-C. Chang, J. M. Williamson, D. W. Cullin, J. R. Dunlop, and T. A. Miller, J. Chem. Phys. **97**, 7999 (1992).
[8] M. I. Lester, R. W. Randall, L. C. Giancarlo, and S. E. Choi, J. Chem. Phys. **99**, 6211 (1993).
[9] M. I. Lester, S. E. Choi, L. C. Giancarlo, and R. W. Randall, Faraday Discuss. (in press).
[10] M.-C. Yang, A. P. Salzberg, B.-C. Chang, C. C. Carter, and T. A. Miller, J. Chem. Phys. **98**, 4301 (1993).
[11] R. W. Randall, C.-C. Chuang, and M. I. Lester, Chem. Phys. Lett. **200**, 113 (1993).
[12] G. W. Lemire, M. J. McQuaid, A. J. Kotlar, and R. C. Sausa, J. Chem. Phys. **99**, 91 (1993). In Table I, the wavenumbers for band F and G for both the (0,0) and (1,0) bands should be interchanged. Additionally, the wavenumbers for band D should read 25 832 and 27 623 cm^{-1}, respectively.
[13] M. J. McQuaid, G. W. Lemire, and R. C. Sausa, Chem. Phys. Lett. **210**, 350 (1993).
[14] E. Hwang and P. J. Dagdigian, J. Chem. Phys. **101**, 2903 (1994).
[15] A. van der Avoird, J. Chem. Phys. **79**, 1170 (1983).
[16] M.-L. Dubernet, D. Flower, and J. M. Hutson, J. Chem. Phys. **94**, 7602 (1991).
[17] W. H. Green Jr. and M. I. Lester, J. Chem. Phys. **96**, 2573 (1992).
[18] M.-L. Dubernet, P. A. Tuckey, and J. M. Hutson, Chem. Phys. Lett. **193**, 355 (1992).
[19] W. M. Fawzy and J. T. Hougen, J. Mol. Spectrosc. **137**, 154 (1989).
[20] C. Chakravarty and D. Clary, J. Chem. Phys. **94**, 4149 (1991).
[21] J. M. Bowman, B. Gazdy, P. Schafer, and M. C. Heaven, J. Phys. Chem. **94**, 2226, 8858 (1990).
[22] U. Schnupf, J. M. Bowman, and M. C. Heaven, Chem. Phys. Lett. **189**, 487 (1992).
[23] M.-L. Dubernet and J. H. Hutson, J. Chem. Phys. **99**, 7477 (1993).
[24] M. I. Lester, R. A. Loomis, L. C. Giancarlo, M. T. Berry, C. Chakravarty, and D. C. Clary, J. Chem. Phys. **98**, 9320 (1993).
[25] A. Degli-Esposti and H.-J. Werner, J. Chem. Phys. **93**, 3351 (1990).
[26] M. H. Alexander, S. Gregurick, and P. J. Dagdigian, J. Chem. Phys. **101**, 2887 (1994).
[27] R. A. Kendall, T. H. Dunning, Jr., and R. J. Harrison, J. Chem. Phys. **96**, 6796 (1992).
[28] K. Bergmann and W. Demtröder, Z. Phys. **243**, 1 (1971).
[29] H. Klar, J. Phys. B **6**, 2139 (1973).
[30] G. C. Nielson, G. A. Parker, and R. T Pack, J. Chem. Phys. **66**, 1396 (1977).
[31] S. Green and R. N. Zare, Chem. Phys. **7**, 62 (1975).
[32] M. H. Alexander, J. Chem. Phys. **76**, 5974 (1982).
[33] M. H. Alexander, Chem. Phys. **92**, 337 (1985).
[34] G. Herzberg, *Spectra of Diatomic Molecules*, 2nd ed. (Van Nostrand, Princeton, 1968).
[35] J. Tennyson and A. van der Avoird, J. Chem. Phys. **77**, 5664 (1984).
[36] J. Hutson, J. Chem. Phys. **89**, 4550 (1988).
[37] B. P. Reid, K. C. Janda, and N. Halberstadt, J. Phys. Chem. **92**, 587 (1988).
[38] D. C. Clary and D. J. Nesbitt, J. Chem. Phys. **90**, 7000 (1989).
[39] J. M. Hutson, in *Advances in Molecular Vibrations and Collision Dynamics*, edited by J. M. Bowman and M. A. Ratner (JAI, Greenwich, CT, 1991), Vol. 1A, p. 1.
[40] J. T. Hougen, J. Chem. Phys. **36**, 519 (1962).
[41] J. M. Brown, J. T. Hougen, K.-P. Huber, J. W. C. Johns, I. Kopp, H. Lefebvre-Brion, A. J. Merer, D. A. Ramsay, J. Rostas, and R. N. Zare, J. Mol. Spetrosc. **55**, 500 (1975).
[42] R. N. Zare, *Angular Momentum* (Wiley, New York, 1988).
[43] M. H. Alexander, H.-J. Werner, and P. J. Dagdigian, J. Chem. Phys. **89**, 1388 (1988).
[44] A. Arthurs and A. Dalgarno, Proc. R. Soc. London Ser. A **256**, 540 (1960).
[45] G. C. Corey and M. H. Alexander, J. Chem. Phys. **85**, 5652 (1986).
[46] M. H. Alexander, J. Chem. Phys. **76**, 3637 (1982).
[47] C. F. Curtiss and F. T. Adler, J. Chem. Phys. **20**, 249 (1952).
[48] P. McGuire and D. J. Kouri, J. Chem. Phys. **60**, 2488 (1974).
[49] R. T Pack, J. Chem. Phys. **60**, 633 (1974).
[50] J. Tennyson and B. T. Sutcliff, J. Chem. Phys. **77**, 4061 (1982).
[51] D. Secrest, J. Chem. Phys. **62**, 710 (1975).
[52] D. J. Kouri, in *Atom–Molecule Collision Theory: A Guide for the Experimentalist*, edited by R. B. Bernstein (Plenum, New York, 1979), p. 301.

[53] S. L. Holmgren, M. Waldman, and W. Klemperer, J. Chem. Phys. **67**, 4414 (1977).
[54] T. H. Dunning, Jr., J. Chem. Phys. **90**, 1007 (1989).
[55] MOLPRO is a package of *ab initio* programs written by H.-J. Werner and P. J. Knowles, with contributions from J. Almlöf, R. Amos, S. Elbert, K. Hampel, W. Meyer, K. Peterson, E. A. Reinsch, R. Pitzer, and A. Stone.
[56] K. P. Huber and G. Herzberg, *Molecular Spectra and Molecular Structure*, Constants of Diatomic Molecules, Vol. IV (Van Nostrand Reinhold, New York, 1979).
[57] S. F. Boys and F. Benardi, Mol. Phys. **19**, 553 (1970).
[58] W. Meyer, Int. J. Quant. Chem. Symp. **5**, 341 (1971).
[59] W. Meyer, J. Chem. Phys. **58**, 1017 (1973).
[60] W. Meyer, Theoret. Chim. Acta **35**, 277 (1974).
[61] H.-J. Werner and P. J. Knowles, J. Chem. Phys. **82**, 5053 (1985).
[62] P. J. Knowles and H.-J. Werner, Chem. Phys. Lett. **115**, 259 (1985).
[63] P. J. Knowles and H.-J. Werner, Chem. Phys. Lett. **145**, 514 (1988).
[64] H.-J. Werner and P. J. Knowles, J. Chem. Phys. **89**, 5803 (1988).
[65] H.-J. Werner and W. Meyer, J. Chem. Phys. **74**, 5794 (1981).
[66] R. N. Diffenderfer and D. R. Yarkony, J. Phys. Chem. **86**, 5098 (1982).
[67] B. H. Lengsfield, J. Chem. Phys. **77**, 4073 (1982).
[68] H.-J. Werner and P. J. Knowles, Theor. Chim. Acta **78**, 175 (1990).
[69] E. R. Davidson and D. W. Silver, Chem. Phys. Lett. **53**, 403 (1977).
[70] Tables of the *ab initio* energies and the expansion coefficients in Eq. (16), as well as a FORTRAN program to determine the radial expansion coefficients $V_\lambda(R)$ in the expansion of V_{sum} and V_{dif} as a function of R are available on request from mha by electronic mail (address: mha@hibridon.umd.edu). Please supply a return electronic mail address.
[71] M. H. Alexander, P.-J. Dagdigian, and H.-J. Werner (unpublished).
[72] Convenience is the only justification for the replacement of Eq. (14) by Eq. (15): the CD bound states calculations are carried out as a special application of our Hibridon inelastic scattering code, which incorporates the centrifugal potential given by Eq. (15). For the CH hydride at low J, the effect of replacing Eq. (14) by Eq. (15) has a negligible effect on the calculated energies.
[73] P. F. Bernath, C. R. Brazier, T. Olsen, R. Hailey, W. T. M. L. Fernando, C. Woods, and J. L. Hardwick, J. Mol. Spectrosc. **147**, 16 (1991).
[74] HIBRIDON is a package of programs for the time-independent quantum treatment of inelastic collisions and photodissociation written by M. H. Alexander, D. E. Manolopoulos, H.-J. Werner, and B. Follmeg, with contributions by P. F. Vohralik, D. Lemoine, G. Corey, B. Johnson, T. Orlikowski, W. Kearney, A. Berning, A. Degli-Esposti, C. Rist, and P. Dagdigian.
[75] J. M. Hutson and B. J. Howard, Mol. Phys. **41**, 1123 (1980); **45**, 769 (1982).
[76] J. M. Hutson, J. Chem. Phys. **89**, 4550 (1988).
[77] W. M. Fawzy, G. T. Fraser, J. T. Hougen, and A. S. Pine, J. Chem. Phys. **93**, 2992 (1990).
[78] S. Fei, X. Zhang, and M. C. Heaven, J. Chem. Phys. **97**, 1655 (1992).
[79] The radial and angular basis sets were extended sufficiently to ensure that no high-lying levels near the Ar–CH dissociation limit were missed.
[80] I. P. Hamilton and J. C. Light, J. Chem. Phys. **84**, 306 (1986).
[81] Y. Ohshima, M. Iida, and K. Endo, J. Chem. Phys. **95**, 7001 (1991).
[82] W. H. Basinger, U. Schnupf, and M. C. Heaven, Faraday Discuss. (in press).